Multianalytical Approach for Deciphering the Specific MS/MS Transition and Overcoming the Challenge of the Separation of a Transient Intermediate, Quinonoid Dihydrobiopterin

Eskander Alhajji, Ayoub Boulghobra, Francis Berthias, Fathi Moussa, Philippe Maître, Myriam Bonose

Multi-analytical approach for deciphering the specific MS/MS transition and overcoming the challenge of the separation of a transient intermediate, quinonoid dihydrobiopterin

Eskander Alhajji, Ayoub Boulghobra, Myriam Bonose, Fathi Moussa, Philippe Maître*

Institut de Chimie Physique, CNRS UMR 8000. Université Paris-Saclay. 91405 Orsay Cedex, France

KEYWORDS. Pterin, tetrahydrobiopterin, quinonoid dihydrobiopterin, transient intermediate.

ABSTRACT: Despite recent technological developments in analytical chemistry, separation and direct characterization of transient intermediates remain an analytical challenge. Among these, separation and direct characterization of quinonoid dihydrobiopterin (qH2Bip), a transient intermediate of tetrahydrobiopterin (H4Bip)-dependent hydroxylation reactions, essential in living organisms, with important and varied human pathophysiological impacts, is a clear illustration. H4Bip regeneration may be impaired by competitive non-enzymatic autoxidation reactions, such isomerization qH2Bip into a more stable 7,8-H2Bip (H2Bip) isomer and subsequent non-enzymatic oxidation reactions. The quinonoid H2Bip intermediate thus plays a key role in H4Bip-dependent hydroxylation reactions. However, only a few experimental results have indirectly confirmed this finding while revealing the difficulty of isolating qH2Bip from H4Bip containing solutions. As a result, no current H4Bip assay method allows this isomer to be quantified even by LC-MS/MS. Here, we report on isolation, structural characterization, and abundance of qH2Bip formed upon H4Bip autoxidation using three methods integrated to tandem mass spectrometry. First, we characterized the structure of the two observed H2B isomers using IR photo-dissociation spectroscopy in conjunction with quantum chemical calculations. Then, we used differential Ion Mobility Spectrometry (DMS) to fully separate all oxidized forms of H4Bip including qH2Bip. The obtained data show that qH2Bip can be unambiguously identified thanks to its specific MS/MS transition. This finding paves the way for the quantification of qH2Bip with MS/MS methods. Most importantly, the half-life value of this intermediate is nearly equivalent to that of H4Bip (tens of min) suggesting that an accurate method of H4Bip analysis should include the quantification of qH2Bip.

Since the elucidation of its pivotal role as cofactor of several essential hydroxylation reactions in living organisms, tetrahydrobiopterin (H4Bip)[1,2] (Fig. 1) raised a considerable interest in the field of human medicine.[3-6] H4Bip synthesis, regeneration, or transport defects are involved in several inborn errors of metabolism including hyperphenylalaninemia, neurotransmitter disorders, and several neurodegenerative disorders such as Alzheimer and Parkinson diseases, autism, and depression.[4] H4Bip defects are also involved in inducible nitric oxide synthase (NOS)-dependent processes, and other important aspects of vascular homeostasis, inflammation, and cardiac function.[4, 5] This ubiquitous pterin also seems to play a growth or proliferation factor role for various cell lines.[4]

The pathophysiology of H4Bip remains an open field of investigation as evidenced by the recent disclosure of a genetic disorder of neurotransmitter translocation into synaptic vesicles[7] or by the renewed interest in its pathophysiological role in vitiligo.[8,9] More recently, H4Bip was also found to be involved in autoimmunity and cancer.[10] It was also suggested that this molecule could be a biomarker for kidney injury in diabetes.[11]

In this context, understanding the origin of H4Bip defects through the characterization of its oxidation pathways (Fig. 1, bottom)[12-16] has always been and remains an important issue from both pathophysiological and diagnostic points of view. [6]

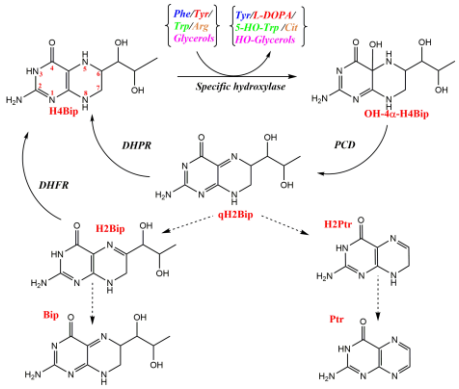

Figure 1: Mechanism of action of tetrahydrobiopterin (H4Bip) (According to refs. 2 – 4). Phe: phenylalanine; Tyr: tyrosine; Trp: tryptophan; Arg: arginine; L-DOPA: di-hydroxy-phenylalanine; OH-Trp: Hydroxy-tryptophan, Cit: citrulline; qH2Bip and H2Bip: quinonoid and 7,8-dihydrobiopterin; Bip: biopterin; H2Ptr: dihydro-pterin; Ptr: pterin. Full arrows denote enzymatic reactions: PCD (pterin-4α-carbinolamine dehydratase), DHPR (dihydro-pteridine reductase), and DHFR (dihydrofolate reductase). Dashed arrows denote non-enzymatic auto-oxidation reactions.

Since pioneering investigations,[2] a consensus has been reached on that H4Bip-dependent hydroxylation reactions (Fig. 1) involve a stoichiometric enzymatic oxidation of H4Bip into quinonoid dihydrobiopterin (qH2Bip). H4Bip is

then regenerated by enzymatic reduction of the latter short-lived intermediate involving a dihydro-pteridine reductase (DHPR).[4]

H4Bip regeneration may be impaired by competitive non-enzymatic autoxidation reactions (Fig. 1). First, part of qH2Bip may rearrange into 7,8-dihydrobiopterin (H2Bip), a more stable isomer as reflected in the increase of the latter in case of DHPR deficiency.[3,4] As shown in Figure 1, autoxidation of H2Bip into biopterin (Bip), and of qH2Bip into dihydropterin (H2Ptr), and pterin (Ptr) may also occur. As a result, quantification of pterins, notably H4Bip, H2Bip, and their precursor dihydro-neopterin (H2N), in biological fluids is of importance for both diagnosis and monitoring of H4Bip supplementation efficacy in patients with genetic defects.[6, 16-21]

The oxidation pathways of H4Bip and the number of intermediates as well as their structures have been questioned.[12,13] The occurrence of qH2Bip as transient intermediate in the H4Bip-dependent hydroxylation reactions was first proposed in 1963.[2] It was later suggested that qH2Bip should be the first product of aerobic or chemical oxidation of H4Bip.[12-14] Only a few attempts have been made to synthesize[22] or to separate and characterize qH2Bip.[17,19] While these attempts indirectly confirmed the occurrence of qH2Bip, it has never been directly characterized.[17-19] Data regarding the half-life of qH2Bip and the stability of H4Bip thus remain scarce and conflicting. First studies suggested that the half-life of this intermediate is very short, but different values were reported, *i.e.* 5 min[17] or from 0.9 to 3.5 min.[22] These values were determined at different pH values and using different buffer types which are known to strongly affect oxidation pathways.[13] In this respect, it has been reported that H4Bip is resistant to oxidation by oxygen at acidic pH,[8] which is particularly unexpected. Finally, in biological samples, H4Bip may oxidize within minutes, without molar relationship between loss of H4Bip and increase of H2Bip and Bip in terms of concentration.[18]

Characterization of qH2Bip following its separation from different oxidation products of H4Bip should provide essential insights into reaction mechanisms involved in H4Bip defects. No current H4Bip assay method including LC-MS/MS methods [20, 21, 23-27] allows this isomer to be quantified. Approaches based on ion mobility spectrometry (IMS) coupled to MS/MS which have been shown to be very efficient for separation and characterization of molecular ions,[29-34] including short-lived intermediates,[28] could thus be interesting for improving the characterization of qH2Bip.

Ion mobility spectrometry (IMS) coupled to MS is currently experiencing considerable development in the field of bioanalysis, notably for metabolite separation and identification.[35] Thanks to the recent development of new commercial ion mobility instruments in both time[36] and space domains[36, 37] and the enhancement of the resolving power by introducing a fraction of He[39] or polar molecules[39-41] in the carrier gas, many challenging separations including separation of isobaric and isomeric species in complex media such as plasma and urine, have been successfully achieved.[35, 42-49]

Among IMS techniques, differential mobility spectrometry (DMS, also referred to as Field Asymmetric waveform Ion Mobility Spectrometry (FAIMS), allows for the reduction of the number of false positive assignments.[31] A great advantage of DMS is that separation of small isomeric molecular ions such as drugs can be achieved through modifier-assisted DMS, *i.e.* by adding polar molecules to the N_2 carrier gas.[38] Coupled to MS/MS, the coverage achieved with DMS is comparable to that achieved with chromatographic methods, while overcoming a low LC resolution resulting in the convoluted MS/MS spectra from isomeric or isobaric species.[42, 43]

Here, we used IR spectroscopy integrated to mass spectrometry, in conjunction with quantum chemical calculations, to prove the presence of both H2Bip isomers and derive their structures. Then, we used DMS coupled to tandem mass spectrometry to fully separate oxidation products of H4Bip including qH2Bip and H2Bip isomers.

EXPERIMENTAL SECTION

Reagents and standards. Bip and H2Bip were purchased from Sigma (Saint-Quentin Fallavier, France). H4Bip was purchased from Schircks Laboratories (Bauma, Switzerland). Standard solutions (10 mM) were prepared in pH 2.5, 0.05 M ammonium formate and immediately aliquoted and frozen at –20 °C. Working solutions were prepared by diluting standard solutions after thawing in the same buffer to a final concentration of 0.1 mM. This sample preparation procedure lasts about 10 min, and the analysis is performed right after. Time 0 thus refers to the 10th min of pre-incubation of the considered pterin working solution.

High resolution tandem mass spectrometry. We used a 7T hybrid FT-ICR (Apex IV, Bruker) instrument equipped with an electrospray ionization (ESI) source. Collision induced dissociation (CID) and infrared multiple photon dissociation (IRMPD) MS^2 experiments were performed. IR activation was provided by an IR OPO/OPA laser (LaserVision), pumped by a non-seeded 25Hz Nd:YAG laser (Innolas Spitlight 600, 550 mJ per pulse, 1064 nm, 4–6 ns pulse duration) as described in detail elsewhere.[50]

IR spectroscopy. IR spectra can be derived from IR MS^2 experiments where mass-selected ions are irradiated for ~500 ms while trapped in the ICR cell.[50] When the IR laser is tuned in resonance with a vibrational mode of a particular isomeric form of the mass-selected ions, fragmentation can be induced following a multiple photon absorption process.[45, 50] Gas phase IRMPD spectra thus correspond to the fragmentation efficiency as a function of the laser wavelength.

Differential mobility tandem mass spectrometry (DMS-MS/MS). DMS-MS/MS experiments were performed using a modified commercial 3D ion-trap (Esquire 3000+, Bruker) instrument equipped with an electrospray ionization (ESI) source. Details on the DMS device and its coupling to the tandem mass spectrometer have been described previously.[50, 51] Briefly, the DMS device is threaded to match the spray shield of the ESI source, such that the spray shield can be removed and the DMS assembly can be screwed on in its place. A 4-kV voltage is applied to the ESI emitter. Ions are transported by a carrier gas stream at atmospheric pressure between two 25 x 6 mm parallel plates, separated by 0.7 mm. Desolvation (N_2) gas, which is redirected through the outer housing of the DMS assembly, serves as carrier gas through the DMS assembly as well as for desolvation when coupled to ESI. For these experiments, temperature of the DMS assembly was about 86 °C.

The standard glass transfer capillary of the source was replaced by a custom flared glass transfer capillary which allows for a better ion transmission.[52]

For DMS separation we used a bi-sinusoidal waveform generated by applying a sinusoidal waveform at 1.7 MHz to one DMS electrode and a second sinusoidal waveform at the second harmonic to the other. [51] The $V_{0\text{-}p}$ defined as the dispersion voltage (DV) was tuned to 1.8 kV (26 kV/cm). A dc offset, termed the compensation voltage (CV), is applied to one electrode allowing transmission of ions of interest through the DMS device based on their differential ion mobility. DMS spectra are generated by plotting ion abundance as a function of CV.

Polar molecules (water, methanol, isopropanol) used as carrier gas phase modifiers [39] are individually delivered (1 to 10 $\mu L.min^{-1}$) into the N_2 gas supply line using a low-flow pumping system (Automatisierung und Microsysteme, CETONI GmbH, GERMANY). The gas line is heated above the boiling point of the modifier thus ensuring a uniform diffusion of the modifier into the carrier gas.

Quantum chemical calculations were performed using the Gaussian09 package.[53] Stationary points on the potential energy surface were characterized at the B3LYP/6-31G(d,p) level of theory. The free enthalpies at 298 K were determined at this same level. IR absorption spectra were derived from harmonic calculations. A scaling factor of 0.955 was applied to harmonic frequencies, as used previously for simulating IR spectra in the X-H (X=C, N, O) stretching spectral range. [50]

RESULTS AND DISCUSSION

The main objective of this work is to isolate and directly characterize native qH2Bip isomer from a solution of H4Bip. We first focused on the evolution of the MS/MS spectra of a fresh H4Bip solution as a function of the incubation time at ambient temperature. Assuming that qH2Bip is the first unstable product of the aerobic oxidation (autoxidation reaction) of H4Bip, which rapidly rearranges to form an H2Bip more stable conformer (Fig. 1), accumulation of the two isomers, as well as subsequent autoxidation products, is expected. Then we used MS/MS(IRMPD) in conjunction with quantum chemical calculations to derive structural information on observed qH2Bip and H2Bip isomers.

High resolution tandem mass spectrometry. Mass spectrum of a 0.1 mM solution of H4Bip, in the positive mode is shown in Figure 2a. Spectral peaks corresponding to protonated Bip, H2Bip, and H4Bip were observed at *m/z* 238, 240 and 242, respectively (Fig. 2a). In order to get more insights on *m/z* 240 ions corresponding to H2B, CID MS^2 spectra were recorded (Fig. 2b, c). As can be seen in Figure 2b, a small peak at *m/z* 220 can be discerned, but the two most abundant product ions were observed at *m/z* 166 and 196. These two ions correspond to the loss of $C_3H_6O_2$ and C_2H_4O, respectively.

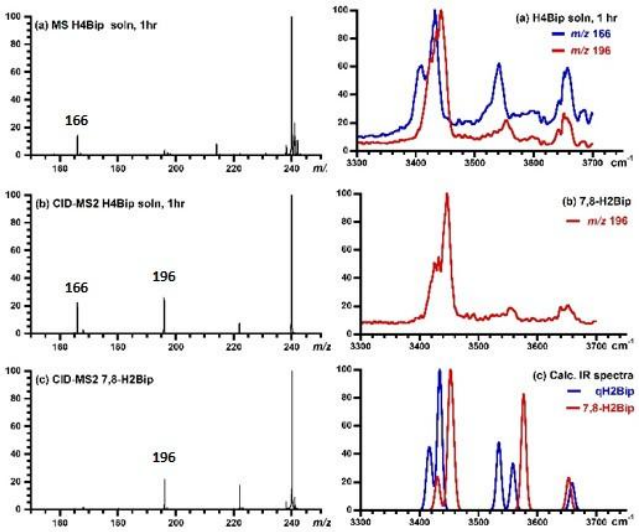

Figure 2: Mass spectra (a-c) and IR spectra (d-f). (a) Mass spectrum of an electrosprayed solution of H4Bip after 1 h of incubation; (b) CID-MS2 spectra of the *m/z* 240 ions corresponding to the H2Bip fragments, recorded after 1 hour of incubation; and (c) CID-MS2 spectrum of an electro-sprayed solution of H2Bip. Experimental IRMPD spectra of (d) the *m/z* 240 ion fragments of an electrosprayed solution of H4Bip after 1 hour of incubation; (e) the *m/z* 240 ions associated with a H2Bip solution, and (f) the calculated IR absorption spectra of the lowest energy isomers of protonated qH2Bip (blue) and H2Bip (red) (see Supplementary Information for more details).

Interestingly, a clear trend of the evolution of the 166/196 intensity ratio as a function of the H4Bip incubation time in the injector (autoxidation reaction) could be observed. As the incubation progresses, there is a gradual decrease in the intensity of the peak at *m/z* 166 concomitantly with the increase in that of the peak at *m/z* 196. This observation suggests that at least two *m/z* 240 isomeric forms are present in solution and transferred to the gas phase.

In order to investigate this hypothesis, CID MS^2 mass spectrum of an electrosprayed standard solution of H2Bip was recorded. As can be seen in Figure 2c, only *m/z* 196 product ions could be observed. Standard long-lived H2Bip isomer is thus characterized by its specific *m/z* 196 fragment. Fragment ion at *m/z* 166 is thus a signature of another isomeric form, which could be qH2Bip ($[qH2Bip+H]^+$ (m/z 240) → m/z 166).

Infrared spectroscopy. Assuming that two protonated H2Bip isomers, $[qH2Bip+H]^+$ and $[H2Bip+H]^+$, are trapped in the ICR cell, infrared spectra of these two *m/z* 240 isomers could be recorded. Using an IR MS^2 sequence, *m/z* 240 ions were mass-selected and then irradiated with the IR laser while trapped in the ICR cell. As shown in scheme 1, m/z 166 (or 196) photo-fragment can only be observed if the IR laser is tuned in resonance with a vibrational mode of $[qH2Bip+H]^+$ or $[H2Bip+H]^+$. As a result, IR spectrum of these two isomeric ions could be recorded by monitoring the fragmentation yield of the two *m/z* 166 and 196 specific product ions, respectively, as a function of the laser wavelength.

The resulting IR spectra recorded under different experimental conditions are shown in Figure 2 (charts d-f). At short autoxidation reaction time (chart d), two distinct IR spectra

could be recorded. At longer autoxidation reaction time, however, only the *m/z* 196 photo-fragment ions could be observed. IR spectra associated with *m/z* 196 photo-fragment ions when recorded at different autoxidation reaction times are similar to the IR spectrum of the *m/z* 240 ions associated with a H2Bip standard solution (Fig. 2e). They are characterized by a strong IR feature with a maximum at 3445 cm^{-1} and a shoulder on its red side. These spectra can be assigned to H2Bip isomer. IR spectra of *m/z* 240 ions associated with *m/z* 166 photo-fragment ions are clearly different. In particular, the maximum of the photo-fragmentation signal is observed at 3435 cm^{-1}. These spectra can be tentatively assigned to qH2Bip tautomer.

Quantum chemical calculations. In order to challenge the above structural assignment quantum chemical calculations have been carried out on the $[qH2Bip+H]^+$ and $[H2Bip+H]^+$ ions. Different protonation sites have been envisaged (Fig. 3). Overall, for both neutral and protonated H2Bip, the most stable structures correspond to H2Bip. The qH2Bip→H2Bip isomerization reaction was found to be exothermic by -62.9 and -75.9 kJ/mol for neutral and protonated systems, respectively. In the case of H2Bip, lowest energy structures correspond to protonation on the N(5) site, while the N(3) is the preferred protonation site for the qH2Bip form. We primarily focused on the assignment of the most intense band observed for the two photo-fragmentation channels which was observed in the 3430-3445 cm^{-1} range.

The most intense IR band predicted for all the lowest energy conformers of the $[qH2Bip+H]^+$ and $[H2Bip+H]^+$ ions corresponds to the symmetric elongation of the amino NH bonds. This band is essentially insensitive to the conformation of the diol side chain. This aliphatic chain is the most flexible part of the systems, and may lead to relatively complicated conformational landscape (Fig. SI1). In this context, an exhaustive conformational search was not required for assigning the two experimental spectra. The position of the symmetric elongation of the amino NH bonds, however, is very sensitive to the conjugation between the amino and the bicyclic group as evidenced by calculated IR absorption spectra.

Theoretical IR absorption spectra of the lowest energy isomers of protonated qH2Bip and H2Bip are given in figure 2f. Consistent with the experimental observation, a blue shift (~15 cm^{-1}) of the symmetric elongation of the amino NH bonds is predicted from protonated H2Bip to qH2Bip structures (Tables SI1 and SI2, respectively). In the case of the IR spectrum associated with *m/z* 166 fragment, a broad and intense band has a maximum at 3435 cm^{-1}, which is the predicted value for the symmetric NH_2 stretching mode of the lowest energy structure of the $[qH2Bip+H]^+$ ion. The maximum of the broad and intense band was observed at 3450 cm^{-1} for the IR spectrum associated with the *m/z* 196 ion, which is in good agreement with the predicted value (3452 cm^{-1}) determined for the symmetric NH_2 stretching mode of the lowest energy structure of the $[H2Bip+H]^+$ ion.

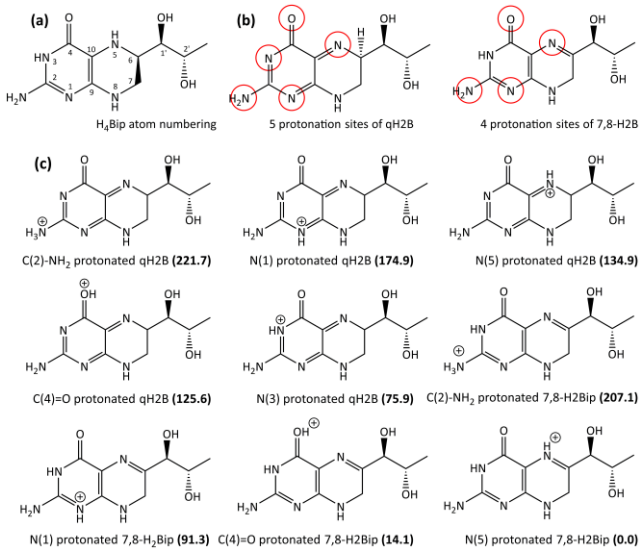

Figure 3: Protonation sites of qH2Bip and H2Bip. (a) Atom numbering for H4Bip; (b) Protonation sites envisaged for each H2Bip tautomer; (c) relative 298K free enthalpies (in kJ/mol), given in bold along with a sketch of the protonated isomer.

Conjugation between the amino and the bicyclic group, *i.e.* electron donation from the former to the latter, is strong in the case of protonated qH2Bip. The driving force for the electron donation of the amino group to the bicyclic group is the stabilization of the positive charge in qH2Bip. This can be illustrated by the resonance of two Kekule-like structures (Scheme 1). Stabilization of the positive charge is evidenced by the calculated $N(3)^+$-H stretching frequency (3414 cm^{-1}) of protonated qH2Bip (Table SI2), which is strongly blue-shifted as compared to that of $N(5)^+$ protonated H2Bip (3268 cm^{-1}) (Table SI1).

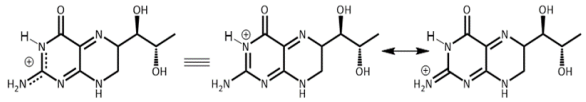

Scheme 1

Considered together, the results obtained by the MS/MS(IRMPD) experiments and the quantum chemical calculations allowed us to identify the two isomers. As the MS/MS transitions are different, these results also show for the first time that MS/MS can be used alone to monitor these two isomers through the multiple reaction (MRM) detection mode. Nevertheless, we used DMS coupled with MS/MS in order to provide more evidence for the existence of the two H2Bip isomers and, most importantly, to overcome the challenge of qH2Bip separation.

Differential mobility spectrometry. DMS-MS has been used to separate qH2Bip from a H4Bip solution incubated at room temperature, and to characterize the lifetime of transient qH2Bip. For this purpose, DMS-MS spectra were recorded over several hours allowing for a relative quantification of H4Bip and its autoxidation products, including qH2Bip, H2Bip, Bip, H2Ptr, and Ptr (Fig. 1). H2Ptr is observed but at a very low level. The evolution of DMS spectra of a H4Bip solution as a function of the incubation time, *i.e.* autoxidation time, is also shown in Figure 4. DMS-MS data were recorded

without and with addition of polar chemical modifier to N_2 carrier gas.

Figure 4a shows the extracted ion chromatograms (XIC) of *m/z* 242, 240, and 238 ions, each displaying a single peak at 0.3 (H4Bip), -0.1 (H2Bip), and -0.2 V (Bip), respectively. With N_2 only as a carrier gas, a single peak labeled H2B is observed irrespective of the DV value. No separation of the targeted *m/z* 240 isomers could be achieved by adding water or methanol in the N_2 carrier gas, irrespective of the flow rate of the chemical modifier (Table SI3).

Addition of IPA in the carrier gas, however, resulted in a significant increase of the peak capacity (Fig. 4b). H4Bip could be clearly resolved from all its oxidation products, especially qH2Bip, and baseline resolution of the two H2B isomers (Fig. 4b) could achieved. One DMS peak is observed at a CV value of -8.5 V (Fig. 4b). It is characterized by the *m/z* 240>166 transition specific of qH2Bip. Conversely, the other DMS peak centered at CV -18.2 V can be assigned to H2Bip based on its specific *m/z* 240>196 transition (Fig. SI2). At the considered incubation time (49 min), two other low intensity peaks corresponding to *m/z* 238 (Bip) and *m/z* 164 (Ptr) are also well resolved (Fig. 4b). As can be seen in figure 4b, a progressive increase of Ptr, Bip, and H2Bip is observed as a function of the incubation time, concomitantly with the decrease of H4Bip and qH2Bip.

DMS-MS experiments at higher IPA flow rates have been performed in order to further improve DMS resolution, but at the expense of sensitivity. The best compromise between resolution and ion transmission is obtained at a flow rate of 5 µl/min (Table SI3). Upon addition of IPA at this flow rate, H2Bip is more shifted (-0.1 to -18.2 V) than qH2Bip (-0.1 to -8.5 V) resulting in a baseline resolution of both isomers (Fig. 4b). Beside resolving these two isomers, we were also interested in resolving qH2Bip and H4Bip that share the *m/z* 166 fragment.

The larger negative CV shift upon IPA addition observed for H2Bip than for qH2Bip can be rationalized considering literature data on the effect of buffer gas modifier such as alcohol molecules on DMS peak position. Clear trends were observed allowing to propose correlations between the strength of the ion-molecule interaction, the magnitude of the negative CV shifts and ion structure.[40] The displacement towards the negative values is greater for stronger ion-molecule interactions. This interaction is strong when the charge is localized and accessible, *e.g.* without steric hindrance. [40, 41] In the present case, the larger negative CV shift observed for H2Bip as compared to qH2Bip can be understood by considering the localization of the electric charge in the two protonated isomers (Fig. 3). As discussed above, the positive charge resulting from the protonation of N(3) of qH2Bip is stabilized by the electronic donation of the amino group (Scheme 1), whereas it is localized in protonated H2Bip (Fig. 3, Tables SI1, and SI2). Thus, the solvation of the ions with isopropanol is more favorable for H2Bip than for qH2Bip, which would explain the weaker CV shift observed for the latter (-8.5 V) than for the former (-18.2 V).

Taken together these results show that addition of IPA in the carrier gas results in the separation of all protonated oxidation products from protonated H4Bip, including H2Bip isomers, Bip, and Ptr with a resolution higher than 1.3 in all instances (Fig. 4b). While the separation of H4Bip and its oxidation products H2Bip, Bip, and Ptr can be easily achieved by current chromatographic methods, this is the first report of separation of qH2Bip from H2Bip.

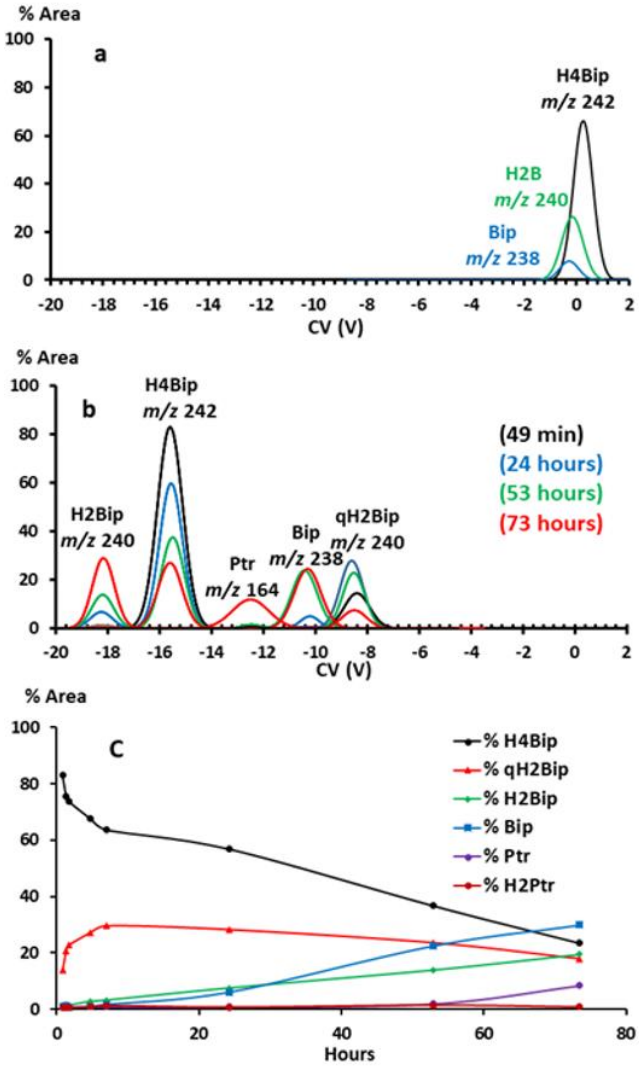

Figure 4: DMS-MS chromatograms (pH 2.3) plotted as a function of the compensation voltage (CV in V), (a) without or (b) with isopropanol (IPA) addition (5 µl.min^{-1}) to the carrier gas (N_2). The mean value of CV standard deviation is 0.1 V. (a) H4Bip, H2Bip, and Bip chromatograms; (b) evolution of relative peak areas as a function of the incubation time, and (c) kinetics of H4Bip autoxidation as a function of the incubation time.

Interesting new insights into the kinetics of autoxidation of H4Bip could also be derived from modifier-assisted DMS-MS experiments. In particular, qH2Bip is still present in the medium at a relatively high percentage (18 %) as compared to H4Bip after 73 hours of incubation at ambient temperature (Fig. 4c, red line). This result questions previous reports where qH2Bip half-life time varies from 0.9 to 3.5 min [26] or 5.0 min [28] at the most. In order to clarify this point, we analyzed further the evolution of the DMS XIC of a fresh H4Bip solution as a function of the incubation time.

As can be seen in figure 4c, H4Bip decreases bi-exponentially with a terminal half-life value of about 40 hours. More precisely, the relative percentage of H4Bip drops to 64 % after 7 hours of incubation, and then slowly decreases to reach about 24 % after 73 hours of incubation. Leaving aside the first minutes of stock solution defrosting and working solution preparation, the half-life value of qH2Bip can be estimated to around 1.7 hours. Although experimental conditions are different, these results are rather consistent with previous reports where, in acidic medium (0.1 mol/l HCl) without antioxidants, a significant fraction of H4Bip is still present after 20 hours of incubation, suggesting that H4Bip half-life value should be on the order of several hours.[18]

At the start of incubation, relative ion population associated with *m/z* 240>166 transition characteristic of qH2Bip is about 14 % of the total peaks area while the relative areas of other oxidation products such as H2Bip, Bip, and Ptr only represent less than 1.5 %, 1 %, and 0.6 %, respectively (Fig. 4c). These products can be attributed to the autoxidation of a fraction of H4Bip during the procedures of preparation/conservation of the stock solutions and preparation/incubation of the working solutions.

The relative area of qH2Bip increases up to about 30 % during the first 7 hours, and then starts to slowly decrease to reach about 18 % at 73 hours (Fig. 4c). After 4.7 hours of incubation, the relative area of the H2Bip peak in turn begins to slowly increase to reach 19.7 % at 73 hours (Fig. 4c). This behavior is consistent with an autoxidation of H4Bip to qH2Bip, which in turn slowly rearranges into H2Bip. Along with the increase of H2Bip, the relative peak area of its autoxidation product Bip simultaneously increases to reach about 30 % at 73 hours. At the end of the experiment, the relative peak area of Ptr, which probably arises from the autoxidation of qH2Bip, reaches about 8 %.

Pioneering work carried out in 1987[18] already showed that H4Bip breakdown at room temperature does not generate equivalent quantities of H2Bip and Bip. Since then, no study added more insights on this point. The data reported herein provide a more complete picture of the autoxidation of H4Bip. In addition to H2Bip and Bip, our results clearly show that the breakdown of H4Bip still produces qH2Bip after several hours of incubation. As qH2Bip is the first oxidation product of H4Bip and as it slowly isomerizes into H2Bip, a significant fraction of qH2Bip is still present after 73 hours of incubation. H4Bip decomposition also leads to pterin release, although at a very low yield (Fig. 4). A precise quantification based on internal standardization will be performed with DMS hyphenated to a triple quadrupole instrument. This work is currently in progress in our laboratory.

The evolution of the abundance of qH2Bip during incubation, at least from 7 to 53 hours, shows the existence of a steady state between its production through autoxidation of H4Bip and its transformation into H2Bip (Fig. 4c). The rate of formation of qH2Bip from autoxidation of H4Bip should thus be very close to that of its conversion to H2Bip (Fig. 4c). Our data also show that the half-life of the qH2Bip conformer is almost equivalent to that of H4Bip, *i.e.* about 1.7 hours under our experimental conditions. This result disagrees with all other previously reported half-lifes varying between 0.9 [26] and 5 min.[17] The observed discrepancies may be attributed to the differences in pH, temperature, and type of buffer as previously suggested.[13] Nonetheless, previous results observed without separation of qH2Bip deserve to be revisited with the proposed method of separation.

CONCLUSIONS

We herein provide evidence that qH2Bip and 7,8-H2Bip isomers can be distinguished based on their MS/MS transitions. In addition, structural information on these isomers is derived from a combination of quantum chemical calculations and infrared photodissociation spectroscopy. From a fundamental point of view, it is important to underline that both DMS and IR data can be simply interpreted by considering the geometrical and electronic structure of both isomers.

Using DMS hyphenated to mass spectrometry, these isomers can be baseline resolved from H4Bip and its other oxidation products, which allows for their quantification. Since qH2Bip half-life is nearly equivalent to that of H4Bip, these results show the importance of integrating the quantification of qH2Bip into current methods of pterins analysis. This would improve the accuracy in terms of diagnosis of H4Bip deficiencies, pharmacokinetics, and therapeutic monitoring, during H4Bip supplementation, as well as quality control of H4Bip-based drugs.

DMS-MS/MS is clearly a valuable alternative separation method for pterins profiling as already proposed for other metabolites.[35, 42-48] An interesting advantage of DMS is that it is a solvent-free separation method. As part of our effort for green chemistry, it can thus be expected that hyphenated to highly sensitive MS/MS instruments such as triple quadrupole ones, ion mobility-based instrument will inexorably complement or even replace current LC-MS/MS methods of molecular analysis.

Supporting Information. Quantum chemical calculations (Fig. SI1, Tables SI1, and SI2), MS/MS spectra (Fig. SI2), and Table SI3 (effects of modifier addition) are supplied as Supporting Information. "This material is available free of charge via the Internet at http://pubs.acs.org."

Corresponding Author

* Philippe Maître. Institut de Chimie Physique, CNRS, Université Paris-Saclay, F-91405, Orsay, France.

Author Contributions

All authors performed research and analyzed the data. P. Maître and F. Moussa designed research and wrote the paper. All authors discussed the data, commented on the manuscript, and have given approval to its final version.

Funding Sources

This work is supported by 3 public grants from the French National Research Agency (ANR) (ANR-10-LABX-0039, ANR-19-CE29-0016-01, and ANR-18-CE09-0042-03). Financial support from the National FT-ICR network (FR 3624 CNRS) for conducting the research is gratefully acknowledged.

REFERENCES

1. Fukuda, T. Conversion of phenylalanine into tyrosine in the silkworm larva (Bombyx mori). *Nature* **1956**, 177(4505):429-30.

2. Kaufman, S. The structure of the phenylalanine-hydroxylation cofactor. *P.N.A.S.* **1963**, 50, 1085–1093.
3. Koslow, S. H.; Butler, I. J. Biogenic amine synthesis defect in dihydropteridine reductase deficiency. *Science* **1977**, 198(4316):522-523.
4. Himmelreich, N.; Blau, N.; b, Thöny, B. Molecular and metabolic bases of tetrahydrobiopterin (BH4) deficiencies. *Molecular Genetics and Metabolism* **2021**, 13, 2, 123-136.
5. Bendall, J. K.; Douglas, G.; McNeill, E.; Channon, K. M.; and Crabtree, M. J. Tetrahydrobiopterin in Cardiovascular Health and Disease. *Antioxidants & Redox Signaling* **2014,** 20 (18), 3040–3077.
6. International Working Group on Neurotransmitter Related Disorders. Consensus guideline for the diagnosis and treatment of tetrahydrobiopterin (BH4) deficiencies. *Orphanet Journal of Rare Diseases* **2020**, 15(1).
7. Rilstone, J. J.; Alkhater, R. A.; and Minassian, B. A. Brain dopamine-serotonin vesicular transport disease and its treatment. *N. Engl. J. Med.* **2013**, 368, 543-550.
8. Telegina, T. A.; Lyudnikova, T. A.; Buglak, A. A.; Vechtomova, Y. L.; Biryukov, M. V.; Demin, V. V.; Kritsky, M. S. Transformation of 6-tetrahydrobiopterin in aqueous solutions under UV-irradiation. *Journal of Photochemistry and Photobiology A: Chemistry* **2018**, 354, 155–162.
9. Buglak, A. A.; Telegina, T. A. Vechtomova, Y; L.; Kritsky, M; S. Autoxidation and photooxidation of tetrahydrobiopterin: a theoretical study. *Free Radical Research* **2021**, 55, 5, 499-509.
10. Cronin, S.J.F.; Seehus, C.; Weidinger, A. *et al.* The metabolite BH4 controls T cell proliferation in autoimmunity and cancer. *Nature* **2018**, 563**,** 564–568.
11. Deng, C.; Wang, S.; Niu, Z.; Ye, Y.; Gao, L. Newly established LC-MS/MS method for measurement of plasma BH4 as a predictive biomarker for kidney injury in diabetes. Free Radical Biology and Medicine **2022,** 178, 1-6.
12. Armarego, W. L. F., Randles, D. and Taguchi, H. Peroxidase catalysed aerobic degradation of 5,6,7,8-tetrahydrobiopterin at physiological pH. *Eur. J. Biochem.* **1983,** 135 393-4031**.**
13. Davis, M. D.; Kaufman, S.; And Milstien, S. The auto-oxidation of tetrahydrobiopterin. *Eur. J. Biochem.* **1988**, 173, 345-351.
14. Kirsch, M.; Korth, H. G.; Stenert, V.; Sustmann, R.; and De Groot, H. The autoxidation of tetrahydrobiopterin revisited. *J. Biol. Chem.* **2003**, 278, 24481–24490.
15. Hoke, K. R.; Crane, B. R. The solution electrochemistry of tetrahydrobiopterin revisited. *Nitric Oxide* **2009**, 20, 79-87.
16. Fukushima, T.; Nixon, J. C. Analysis of Reduced Forms of Biopterin in Biological Tissues and Fluids. *Anal. Biochem*. **1980**, *102*, 176–188.
17. Haavik, J.; Flatmark, T. Isolation and Characterization of Quinonoid Dihydropterins by High-Performance Liquid Chromatography. *J. Chromatogr.* **1983**, 251, 36 –372.
18. Howells, D. W.; Hyland, K. Direct analysis of tetrahydrobiopterin in cerebrospinal fluid by high-performance liquid chromatography with redox electrochemistry: Prevention of autoxidation during storage and analysis. *Clin Chim Acta* **1987**, 167, 23-30. 21.
19. Heales, S.; Hyland, K. Determination of quinonoid dihydrobiopterin by high-performance liquid chromatography and electrochemical detection**.** *J. Chromatogr. Biomed. Appl.* **1989**, 494, 77-85.
20. Guibal, P.; Lo, A.; Maitre, M.; and Moussa, F. Pterin determination in cerebrospinal fluid: state of the art. *Pteridines* **2017**, 28(2): 83–89.
21. Jung-Klawitter, S.; and Hübschmann, O. K. Analysis of Catecholamines and Pterins in Inborn Errors of Monoamine Neurotransmitter Metabolism—From Past to Future. *Cells* **2019**, 8, 867.
22. Matsuura, S.; Murata, S.; Sugimoto, T. Quinonoid dihydrobiopterin, an important metabolic intermediate of biopterin cofactor in the aromatic hydroxylation of amino acids. *Tetrahedron Letters* **1986**, 27, 5, 585-588.
23. Guibal, P.; Le, N.; Doummar, D.; Giraud, N.; Roze, E.; Rodriguez, D.; Couderc, R., Billette De Villemeur, T.; Moussa, F. Simultaneous determination of all forms of biopterin and neopterin in cerebrospinal fluid. *ACS Chemical Neuroscience* **2014**, 5 (7), 533–541.
24. Fismen, L.; Eide, T.; Djurhuus, R.; Svardal, A. M. Simultaneous quantification of tetrahydrobiopterin, dihydrobiopterin, and biopterin by liquid chromatography coupled to electrospray tandem mass spectrometry**.** *Analytical Biochemistry* **2012**, 430, 163–170**.**
25. Burton, C.; Shi, H.; Ma, Y. Development of a high-performance liquid chromatography – tandem mass spectrometry urinary pterinomics workflow. *Analytica Chimica Acta* **2016**, 927, 72-81.
26. Xiong, X.; Liu, Y. Chromatographic behavior of 12 polar pteridines in hydrophilic interaction chromatography using five different HILIC columns coupled with tandem mass spectrometry. *Talanta* **2016**, 150, 493-502.
27. Arning, E.; Bottiglieri, T. LC-MS/MS Analysis of Cerebrospinal Fluid Metabolites in the Pterin Biosynthetic Pathway. *JIMD Rep.* **2016**, 29: 1-9.
28. Zhang, J. T.; Wang, H. Y.; Zhang, X.; Zhang, F.; and Guo, Y. L. Study of short-lived and early reaction intermediates in organocatalytic asymmetric amination reactions by ion-mobility mass spectrometry. *Catal. Sci. Technol.* **2016**, 6, 6637-6643**.**
29. Both, P.; Green, A. P.; Gray, C. J.; Sardzik, R.; Voglmeir, J.; Fontana, C.; Austeri, M.; Rejzek, M.; Richardson, D.; Field, R. A.; Widmalm, G.; Flitsch, S. L.; Eyers, C. E. Discrimination of epimeric glycans and glycopeptides using IM-MS and its potential for carbohydrate sequencing**.** *Nature Chemistry* **2014,** *6*, 65–74.
30. Lanucara, F.; Holman, S. W.; Gray, C. J.; Eyers, C. E. The power of ion mobility-mass spectrometry for structural characterization and the study of conformational dynamics**.** *Nature Chemistry* **2014,** *6*, 281-294.
31. Schneider, B.B.; Nazarov, E.G.; Londry, F.; Vouros, P.; and Covey, T.R. Differential mobility spectrometry/mass spectrometry history, theory, design optimization, simulations, and applications. *Mass Spectrom. Rev.* **2016**, 35, 687-737.
32. Baird, M. A.; Anderson, G. A.; Shliaha, P. V.; Jensen, O. N.; and Shvartsburg, A. A. Differential Ion Mobility Separations/Mass Spectrometry with High Resolution in Both Dimensions. *Anal. Chem.* **2019**, 91, 1479−1485.
33. Bohnhorst, A.; Kirk, A. T.; and Zimmermann, S. Toward Compact High-Performance Ion Mobility Spectrometers: Ion Gating in Ion Mobility Spectrometry. *Anal. Chem.* **2021**, 93, 15, 6062–6070.
34. Rüger, C. P.; Le Maître, J.; Maillard, J.; Riches, E.; Palmer, M.; Afonso, C.; Giusti, P. Exploring Complex Mixtures by Cyclic Ion Mobility High-Resolution Mass Spectrometry: Application Toward Petroleum. *Anal. Chem.* **2021**, 93(14), 5872-5881.
35. Paglia, G.; and Astarita, G. Metabolomics and lipidomics using traveling-wave ion mobility mass spectrometry. *Nature Protocols* **2017**, 12, 797-813.
36. Fernandez-Lima, F.A.; Kaplan, D.A.; and Park, M.A. Note: Integration of trapped ion mobility spectrometry with mass spectrometry. *Rev. Sci. Instrum.* **2011**, 82(12): 126106.
37. Webb, I. K.; Garimella, S. V. B.; Tolmachev, A. V.; Chen, T. C.; Zhang, X. Y.; Norheim, R. V.; Prost, S. A.; LaMarche, B.; Anderson, G. A.; Ibrahim, Y. M.; and Smith, R. D. Experimental evaluation and optimization of structures for lossless ion manipulations for ion mobility spectrometry with time-of-flight mass spectrometry**.** *Anal. Chem.* **2014**, 86, 9169-9176.
38. Ruskic, D.; Hopfgartner, G., Modifier Selectivity Effect on Differential Ion Mobility Resolution of Isomeric Drugs and Multidimensional Liquid Chromatography Ion Mobility Analysis. *Anal. Chem.* **2019,** *91* (18), 11670-11677.
39. Porta, T., Varesio, E.; and Hopfgartner, G. Gas-Phase Separation of Drugs and Metabolites Using Modifier-Assisted Differential Ion Mobility Spectrometry Hyphenated to Liquid Extraction Surface Analysis and Mass Spectrometry. Anal. Chem. **2013**, 85(24): 11771-11779.

40. Campbell, J. L.; Zhu, M.; Hopkins, W. S.: Ion-molecule clustering in differential mobility spectrometry: lessons learned from tetraalkylammonium cations and their isomers. *J. Am. Soc. Mass Spectrom.* **2014**, 25, 1583–1591.
41. Liu, C.; Le Blanc, J.C.Y.; Shields, J.; Janiszewski, J.S.; Ieritano, C.; Ye, G.F.; Hawes, G.F.; Hopkins, W.S.; Campbell, J.L.: Using differential mobility spectrometry to measure ion solvation: an examination of the roles of solvents and ionic structures in separating quinoline-based drugs. Analyst **2015**, 14, 6897–6903.
42. Lintonen, T. P. I.; Baker, P. R. S.; Suoniemi, M.; Ubhi, B. K.; Koistinen, K. M.; Duchoslav, E.; Campbell, J. L.; and Ekroos, K. Differential mobility spectrometry-driven shotgun lipidomics. *Anal. Chem.* **2014**, 86, 9662-9669.
43. Jonasdottir, H. S.; Papan, C.; Fabritz, S.; Balas, L.; Durand, T.; Hardardottir, I.; Freysdottir, J.; and Giera, M. Differential mobility separation of leukotrienes and protectins**.** *Anal. Chem.* **2015**, 87, 5036-5040.
44. Fouque, K.J.D.; Garabedian, A.; Porter, J.; Baird, M.; Pang, X.Q.; Williams, T.D.; Li, L.J.; Shvartsburg, A.; and Fernandez-Lima, F. Fast and effective ion mobility - mass spectrometry separation of D-amino acid containing peptides. *Anal. Chem.* **2017**, 89, 11787-11794.
45. Berthias, F.; Maatoug, B.; Glish, G. L.; Moussa, F.; Maitre, P. Resolution and assignment of differential ion mobility spectra of sarcosine and isomers. *J Am Soc Mass Spectrom.* **2018**, 29(4), 752-760.
46. Perez-Miguez, R.; Bruyneel, B.; Castro-Puyana, M.; Marina, M.L.; Somsen, G.W.; and Dominguez-Vega, E. Chiral discrimination of dl-amino acids by trapped ion mobility spectrometry after derivatization with (+)-1-(9-fluorenyl)ethyl chloroformate. *Anal. Chem.* **2019**, 91, 3277-3285.
47. Winter, D. L.; Mastellone, J.; Kabir, K. M. M.; Wilkins, M. R.; and Donald, W. A. Separation of isobaric mono- and dimethylated RGG-repeat peptides by differential ion mobility-mass spectrometry. *Anal. Chem.* **2019**, 91, 11827-11833.
48. Berthias, F.; Wang, Y.; Alhajji, E.; Rieul, B.; Moussa, F.; Benoist, J.F.; and Maître, P. Identification and quantification of amino acids and related compounds based on Differential Mobility Spectrometry. Analyst **2020**, 145 (14), 4889-4900.
49. Berthias, F.; Baird, M.A.; Shvartsburg, A.A. Differential Ion Mobility Separations of d/l Peptide Epimers. Anal Chem. **2021**; 93(8):4015-4022.
50. Bakker, J. M.; Sinha, R. K.; Besson, T.; Brugnara, M.; Tosi, P.; Salpin, J. Y.; Maitre, P. Tautomerism of uracil probed via IR spectroscopy of singly hydrated uracil. *J. Phys. Chem. A* **2008,** *112*, 12393–12400.
51. Hernandez, O.; Isenberg, S.; Steinmetz, V.; Glish, G. L.; Maitre, P. Probing mobility-selected saccharide isomers: selective ion–molecule reactions and wavelength-specific IR activation**.** *J. Phys. Chem. A* **2015,** *119*, 6057–6064.
52. Bushey, J. M.; Kaplan, D. A.; Danell, R. M.; Glish, G. L. Pulsed nano-electrospray ionization: characterization of temporal response and implementation with a flared inlet capillary**.** *Instrum. Sci. Technol.* **2009,** *37*, 257–273.
53. Frisch, M.J., Trucks, G.W., Schlegel, H.B., et al. Gaussian 09. Gaussian, Inc., Wallingford (**2009**).

Table of contents